Preparation and Characterization of Biobased Graphene from Kraft Lignin

Fu Liu, Yao Chen* and Jianmin Gao*

Graphene was manufactured from commercial kraft lignin, and its forming mechanism, structure, and properties were investigated. A single factor test was employed to determine the optimum conditions of the production of graphene nanosheets. Kraft lignin was mixed with iron powders as catalyst with different weight ratios. The mixed carbon source and catalyst were thermally treated at 1000 °C and incubated for a period of time in a tubular furnace. The thermally treated carbon materials were analyzed by field emission scanning electron microscopy (FE-SEM), Raman spectroscopy, atomic force microscopy (AFM), Fourier transform infrared spectroscopy (FTIR), and X-ray diffraction (XRD). The preferable conditions for production of graphene nanosheets from kraft lignin were determined. The graphene fold structure was obtained after thermally treating for 90 min when the ratio of carbon source to iron was 3:1. The results revealed that folded lamellar graphene structure increased with greater holding time. Carbon nanotubes (CNTs) were observed after thermal treatment for 105 min. These results indicate the formation of graphite crystal structure and multi-layered graphene from kraft lignin in the presence of iron catalyst.

Keywords: Biobased graphene; Kraft lignin; Preparation; Characterization

*Contact information: MOE Key Laboratory of Wooden Material Science and Application, Beijing Forestry University, Beijing, P. O. Box 100083, China; *Corresponding author: jmgao@bjfu.edu.cn; ychen@bjfu.edu.cn*

INTRODUCTION

Kraft lignin is a high-volume byproduct from the pulping industry. Most lignin is not isolated, and the complex structure of lignin makes the production of value-added chemicals difficult. Kraft lignin is an undervalued product that has not yet provided economic returns. Typically, it is burned to recover pulping chemicals and provide steam for power production. Finding value-added applications of kraft lignin is necessary to achieve economic and environmental benefits. Kraft lignin is a carbon-rich material containing guaiacyl (G-type) and syringyl (S-type) structure units. The structure of each carbon atom in a benzene ring is sp^2 hybridized, which is the basic unit of graphene. It is meaningful to turn low-cost kraft lignin into value-added carbon-based nanomaterials such as graphene. Considerable efforts have focused on utilizing waste lignin as one of the components in polymer matrices for high performance composite applications (Thakur *et al.* 2014). However, there are few reports on the efficacious conversion of kraft lignin to graphene. Graphene sheets have been extensively studied due to their unique properties such as excellent electrical (Wei *et al*. 2009) and thermal conductivity (Chen *et al*. 2012), optical (Loh *et al*. 2010), mechanical (Rafiee *et al*. 2009), and chemical properties (Park *et al*. 2008). However, production of graphene uniformly in large-scale with high-quality is still a bottleneck for graphene application (Liang *et al*. 2016).

The methods of graphene preparation at large scale are oxidation-reduction and chemical vapor deposition (CVD). Many strong oxidizers and reducing agents are used in the oxidation-reduction method; such reagents are toxic and hazardous to the environment and human health. Moreover, the product quality is poor due to the defects and residual functional groups introduced during the severe oxidation and reduction processes. Chemical vapor deposition meets the requirements of both large-scale and high quality (Vlassiouk *et al*. 2013). However, graphene transfer is difficult. Metal substrates are recalcitrant to etching and recycling. One proposed method is solid carbon sources metal catalysis, which needs less resources and has an easier operation than other methods. For example, high quality pristine graphene has been prepared from 10 mg of finely ground fluorene ($C_{13}H_{10}$) and sucrose powder as a carbon source (Sun *et al*. 2010). Mun *et al*. (2013a) prepared graphene nanosheets using sodium lignosulfonate as a solid carbon source and iron nanoparticles as a catalyst; the iron nanoparticles were removed by magnetic separation (2013b). Other biomass materials are potential solid carbon sources for graphene fabrication. Graphene growth can be initiated by metal catalysts (Fujita *et al*. 2009; Juang *et al*. 2009; Rodríguez-Manzo *et al*. 2011). The operation is simple, but the purity is low. Metal catalysts cannot be fully removed by chemical treatment. Graphene growth is typically divided into two categories, where the focus is on (i) obtaining a single layer of high quality graphene or (ii) developing a cheap method to obtain multi-layer graphene that can be dispersed, if needed to be, in a solution to create a composite. Preparation of biobased graphene from kraft lignin is closely linked to the latter aim.

The objective of this study was to prepare graphene using commercial kraft lignin as a solid carbon source and to explore the optimum preparation conditions. The effect of holding time and catalyst ratios on graphene formation was evaluated. Field emission scanning electron microscopy (FE-SEM), Raman spectroscopy, atomic force microscopy (AFM), Fourier transform infrared spectroscopy (FTIR), and X-ray diffraction (XRD) were used to characterize the thermal treated samples.

EXPERIMENTAL

Materials

Kraft lignin from an alkaline pulping process was used as solid carbon source. It was obtained from a pilot plant in Beijing, China. Iron powder of AR grade (Beijing Chemical works, Beijing, China) was used as the catalyst for the thermal treatment. A commercial industrial grade graphene were bought from Jining leader-Nano Technology Co., Ltd. All chemicals were of analytical grade and used as received.

Thermal Treatment

Thermal treatment was carried out in an electric tube furnace (SK-G08123K-2-420) equipped with a mass flow controller (ZL-03H) and vacuum control system (ZX-02A). For each experimental run, 5 g of kraft lignin with various weight ratios of Fe powder (Fe/KL 1:2, 1:3, 1:5, 1:7) were mixed and loaded into the quartz tube. Before thermal treatment, the air in the quartz tube was removed by vacuum followed by argon flow. The sample was heated to 1000 °C at a ramping rate of 10 °C/min with a flow of 300 cubic centimeters per minute Ar. The temperature was held at 1000 °C for 60, 75, 90, 105, or 120 min. After thermal treatment, the sample was cooled to room temperature under an argon atmosphere. The air vent valves were closed simultaneously to exclude outside air. The obtained carbon

materials were rinsed with de-ionized water several times. Iron particles were removed by magnetic separation. Finally, the carbon materials were washed with 10% HCl to remove residual iron, filtered, neutralized, and vacuum dried at room temperature.

Characterization

The surface morphology of the carbon materials was analyzed using a field emission scanning electron microscope (JEOL JSM-7001F, Tokyo, Japan). The micro-structure of the carbon materials was analyzed *via* the Raman spectra, recorded using a Lab RAM HR800 spectrometer (Horiba, Japan). A He-Ne laser (532 nm) was the excitation source. Backscattered Raman signals were collected through a microscope and holographic notch filters in the range of 3000 to 1000 cm^{-1} with a spectral resolution of 2 cm^{-1}. Atomic force microscope observation of graphene nanosheets was performed on a Bruker Multimode 8 scanning probe microscope (Karlsruhe, Germany) in tapping mode with silicon tips. The graphene nanosheets were dispersed in anhydrous ethanol and dip-coated onto mica surfaces before testing. The samples were tested before and after thermal treatment on a Thermo Scientific Nicolet TM6700 FTIR spectrometer (Thermo Nicolet Corporation, Waltham, MA, USA). For each sample, 64 scans were recorded from 4000 to 650 cm^{-1} with a resolution of 4 cm^{-1}. Powder X-ray diffraction (XRD) was performed with a Bruker D8 Advance X-ray diffractometer using Cu Ka radiation. The scanning angle was 5 to 30°, and the step size was 0.008°.

RESULTS AND DISCUSSION

FE-SEM Analysis

FE-SEM images of the carbon materials obtained with Fe/KL 1:3 and different holding times are shown in Fig. 1.

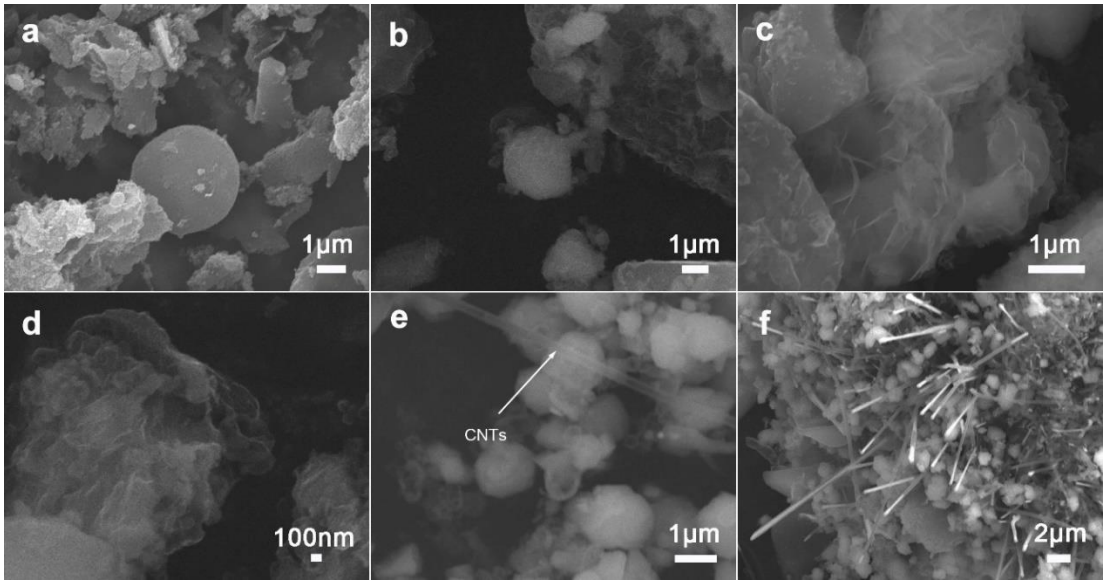

Fig. 1. FE-SEM images of thermal treated carbon materials produced with various holding times. (a) 75 min; (b) 90 min, an iron particle was coated by carbon materials; (c) 90 min, folded and imbricated structure of graphene; (d) 90 min, the morphologies of multilayer lignin-based graphene; (e) 105 min; (f) 120 min

When thermal treatment temperature and holding time were held constant, the amount of graphene layer structure increased with increased catalyst concentration. Amorphous carbon existed as sheets, and solids with larger pieces were the main products when the holding time was 75 min (Fig. 1a). This result suggested that graphitization did not occur to an appreciable extent up to 75 min. The iron particles were not fully encapsulated. A graphene sheet with a multi-layer stacked lamellar and agglomerate structure is shown in Fig. 1c and 1d. There was an abundance of folded lamellar structure that appeared at 90 min. The amount of graphene sheet increased with the holding time increasing to 105 min. However, graphene sheets became agglomerative, and some carbon nanotubes (CNTs) formed (Fig. 1e).

The amount of CNTs increased with the increase in holding time to 120 min (Fig. 1f). Some of the CNTs grew on the iron particles, and some arose from agglomerated graphene. The formation of CNTs could be attributed to the catalysis of iron particles and the decrease of vacuum degree in quartz tube during the cooling process. The graphene–CNTs system has significant technological advantages due to the combination of individual properties of graphene and CNTs in various applications (Kalita *et al*. 2008; Rodríguez-Manzo *et al*. 2009; Lee *et al*. 2010; Zhang *et al*. 2011).

Raman Spectroscopy Analysis

To explore the effect of catalyst proportions on the properties of graphene nanosheets, the Raman spectra of the carbon materials produced with different Fe/KL ratios holding for 90 min were examined (Fig. 2). There were strong defects in the D peak at 1300 cm^{-1}, G peak at 1580 cm^{-1}, and a small 2D peak at 2700 cm^{-1}, which are characteristic peaks of graphene. The broad peak around 2800 cm^{-1} to 3000 cm^{-1} is the D+D′ peak (Tan *et al*. 2001), which represents a vibrational phase of biphonon in disordered crystals (Vallée *et al*. 1988). This result indicated the disordered crystals of the carbon material. The D peak represents lattice defects of C atoms, while the G peak is related to vibration of sp^2-bonded carbon atoms in a two-dimensional hexagonal lattice (Fan *et al*. 2014).

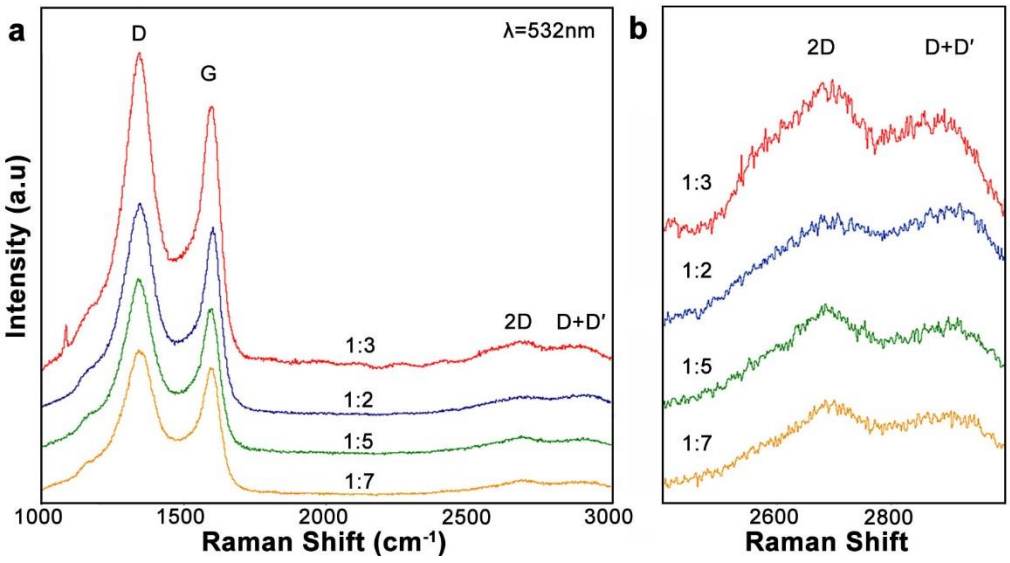

Fig. 2. (a) Raman spectra of graphene produced with various catalyst proportions; (b) is an enlarged partial view of (a).

The peak intensity ratio of D peak to G peak (I_D/I_G) as a defect density was calculated and shown in Table 1. There was no obvious difference in the values obtained with different Fe/KL ratios. Thus, defect density was seldom affected by the catalyst proportions. The 2D peak is the second order of D peak, which is caused by dual vibration of Raman scattering. The D peak is sensitive to the number of graphene layers (Zhao *et al*. 2010). The peak intensity ratio of G peak to 2D peak (I_G/I_{2D}) is positively correlated to the number of graphene layers (Reina *et al*. 2008). Graphene is unstable due to the large specific surface area. Graphene will reduce its own energy through spontaneous agglomeration. When dried, the graphene powder became very agglomerated, leading to no significant increment in Raman 2D peak. The intensity of the 2D peak was relatively higher when the Fe/KL ratio was 1:3, which suggested that thinner graphene with less agglomeration was produced when Fe/KL was 1:3.

Table 1. Intensity of Raman Shift and Ratios of Graphene Produced with Different Fe/KL

Fe/KL Ratio	I_D	I_G	I_{2D}
1:3	6169	5291	1477
1:2	3671	3281	-
1:5	3062	2571	484
1:7	2548	2237	423

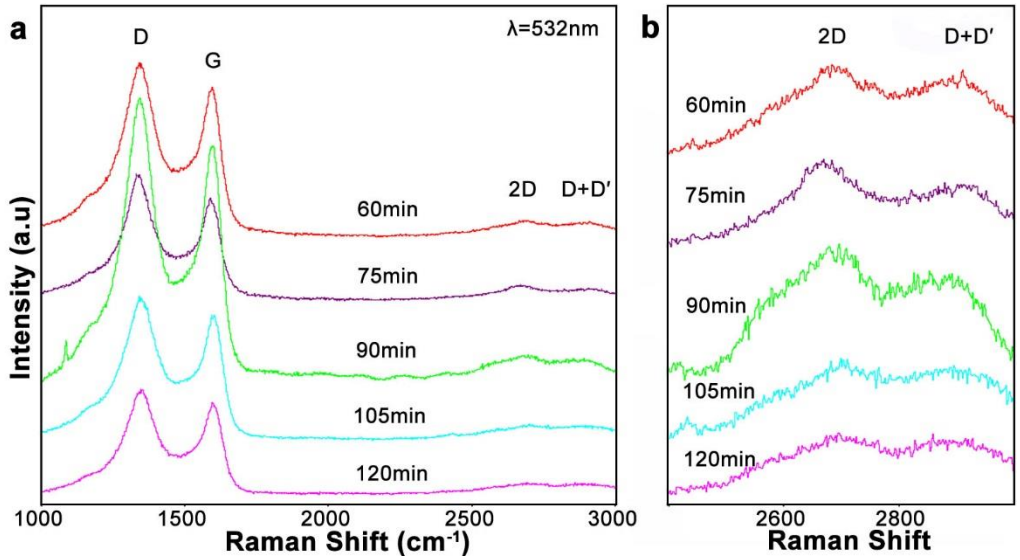

Fig. 3. (a) Raman spectra of graphene with different holding times; (b) is an enlarged partial view of (a).

To evaluate the influence of holding time on the properties of graphene nanosheets, the Raman spectra of the carbon materials produced with Fe/KL 1:3 and holding for 60 min, 75 min, 90 min, 105 min, and 120 min are shown in Fig. 3. There was no obvious difference in I_D/I_G values of the carbon materials treated with different holding times. Therefore, the defect density depended less on holding time during thermal treatment. The value of I_G/I_{2D} was lower when the holding time was 90 min (Table 2). This result indicated that graphene with fewer layers was produced at 90 min.

Table 2. Intensity of Raman Shift and Ratios of Graphene Produced with Different Holding Times

Holding Time	I_D	I_G	I_{2D}
60 min	3400	2955	527
75 min	2461	2015	439
90 min	6169	5291	1477
105 min	2799	2458	470
120 min	2126	1870	410

AFM Analysis

Atomic force microscopy is a powerful means to investigate the lamellar structure of graphene, as it quantifies graphene layers directly and efficiently. The measured thickness is larger than the actual thickness due to the presence of surface species or impurities. Undulations on a graphene surface dried on the mica substrate will also increases its apparent thickness (Si and Samulski 2008). AFM was used to observe the thermal treated sample (Fe:KL = 1:3, holding time = 90 min) dispersed in alcohol. The thickness of monolayer graphene on mica surfaces is often between 0.5 and 1 nm. The surface profile along the white line (1, 2) in Fig. 4(a) shows that the spots have heights as high as approximately 4 nm (Fig. 4 b and 4c), which typically corresponds to four to eight layers of graphene (Novoselov *et al*. 2005; Lui *et al*. 2009). This result indicated that the graphene nanosheets had few layers, which was consistent with the primary analysis.

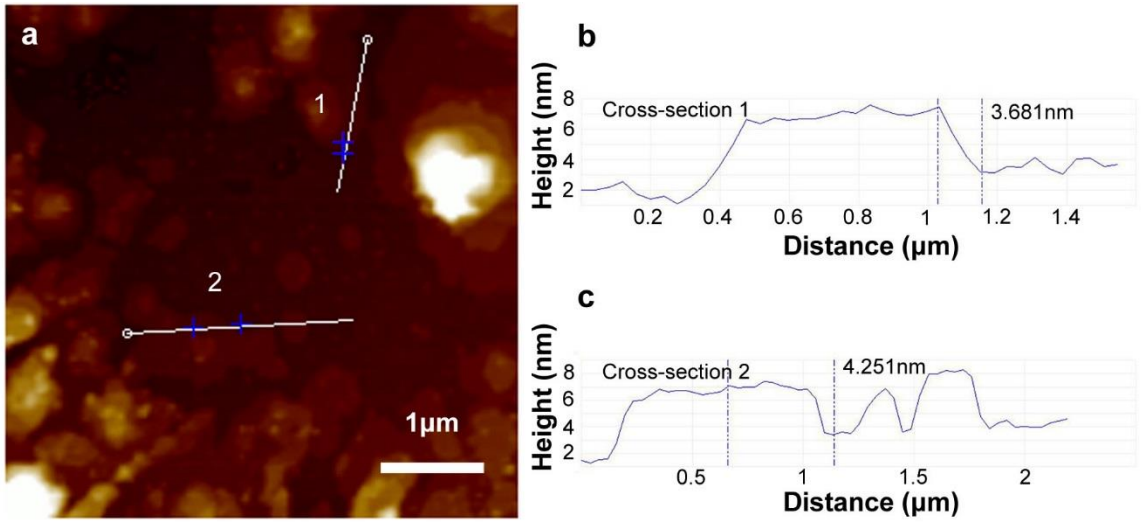

Fig. 4. Atomic force microscope image of the carbon materials obtained with Fe/KL 1:3 and holding time was 90 min. (b), (c) Height profile of the surface measured along the white line in (a).

FTIR Spectroscopy Analysis

FTIR was used to analyze and characterize the chemical structures of the thermal treated sample. The FTIR spectra of the KL and Fe/KL (1:3) after being subjected to thermal treatment for 90 min is shown in Fig. 5. The characteristic peaks of lignin at 1461 cm^{-1}, 1517 cm^{-1}, and 1610 cm^{-1} disappeared after thermal treatment. A peak at 1630 cm^{-1} appeared for the thermal treated sample, which is assigned to the C = C skeletal vibration of graphene sheets (Szabó *et al*. 2005). The broad peak at about 1050 cm^{-1} for the thermal treated sample is attributed to alkoxy (C - O) stretching vibration. These results confirmed the formation of graphene-like materials in the presence of an iron catalyst.

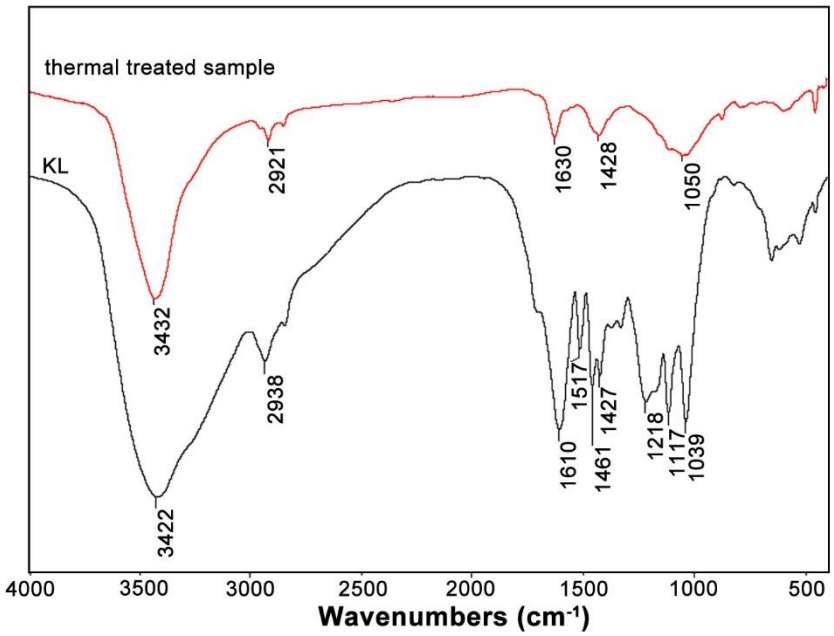

Fig. 5. FTIR spectroscopy of KL and the thermal treated carbon materials

XRD Analysis

XRD was preformed to study the crystal structure of graphene sheets in the annealed sample. The curve-fitting patterns between 17° to 29° of the KL thermal treated for 90 min with Fe/KL 1:3 were illustrated in Fig. 6. The XRD spectrum of the thermal treated sample after magnetic separation, washing with HCl solution (10%) and deionized water, displayed a strong and sharp X-ray diffraction peak at around 26.5°. Hence, the produced graphite had a high degree of crystallization.

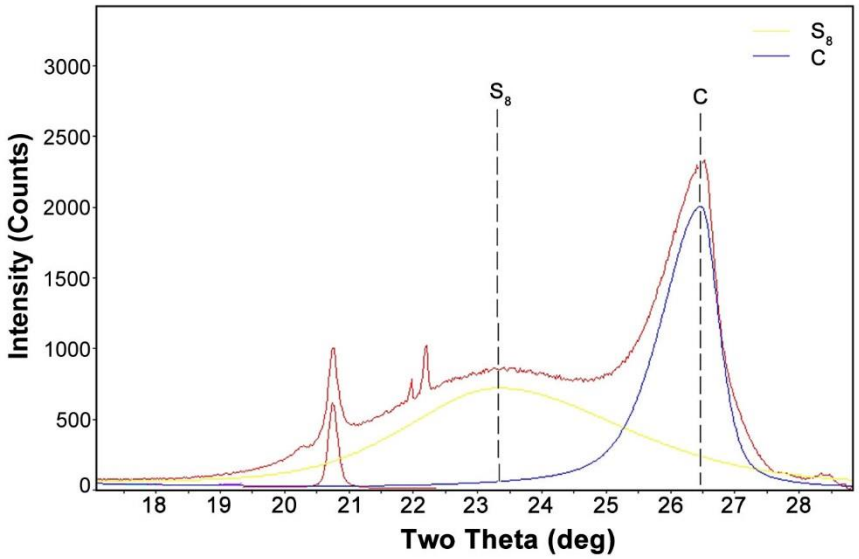

Fig. 6. XRD peak fitting curves of KL thermally treated with Fe particles

The precipitated phases were mainly composed of graphite-2H. The 2H phase is

single layer graphite in the order of AB Bernal stacking (Shi *et al*. 1997). The broad peak at about 23.6° is identified as S8, which originated from the chemicals used during pulping.

Comparison of the Biobased Graphene with the Commercial Graphene

A commercial thermally reduced specimen of graphene oxide (r-GO) was purchased to compare with the biobased graphene. The r-GO had a more prominent 2D peak than biobased graphene, as shown in Fig.7(a). It is apparent that the r-GO had a number of graphene layers stacked and that the stacks were more structured. Due to differences in preparation of raw materials, the r-GO had no sulfur impurities in it (Fig.7b). Compared with the biobased graphene, the r-GO had more carbon-oxygen bonds (Fig.7c). The atomic force microscope image showed that the r-GO had less layers than biobased graphene (Fig.7d). However, there were also many impurities in r-GO.

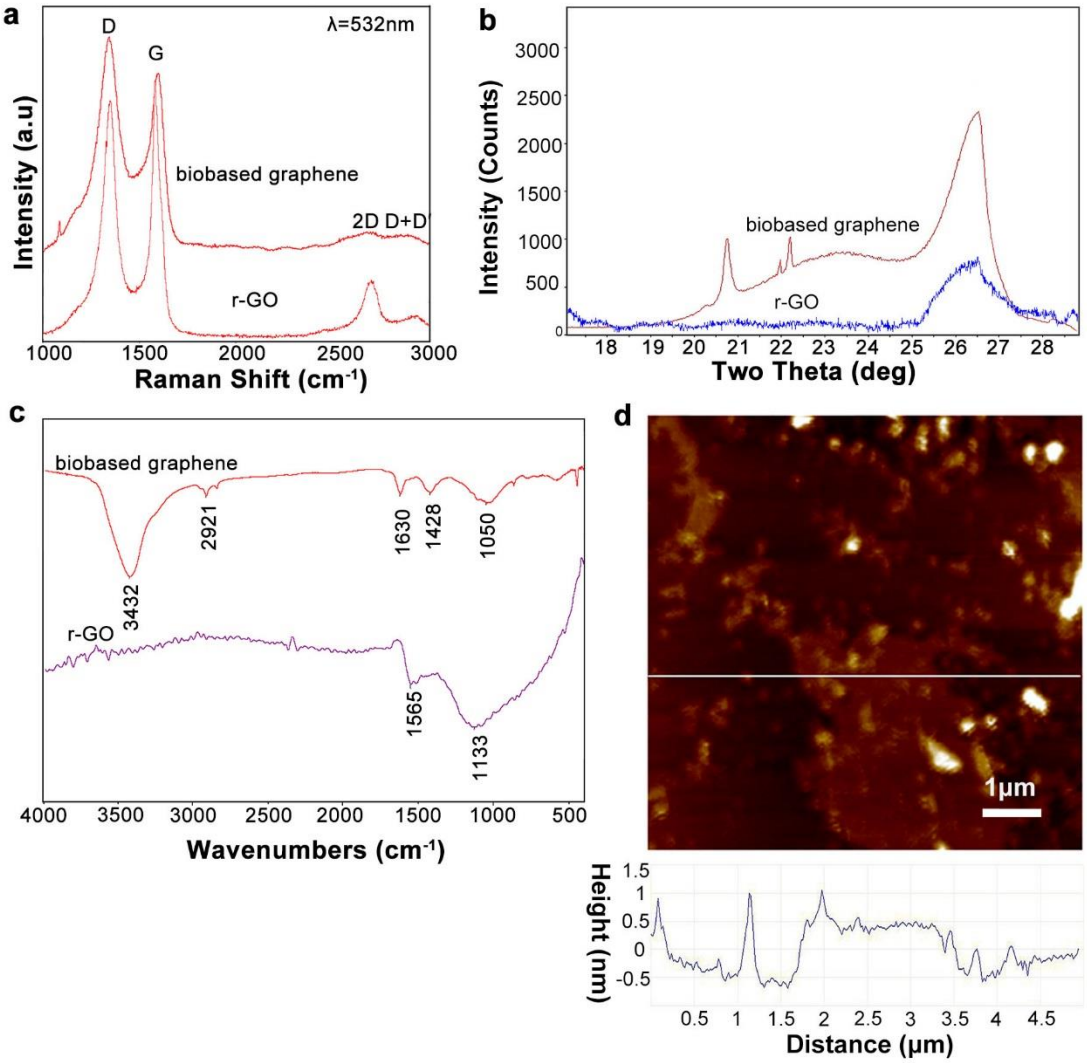

Fig. 7. Comparison of the biobased graphene with the commercial graphene (a) Raman spectroscopy; (b) X-ray diffraction pattern; (c) FTIR spectroscopy; (d) Atomic force microscope image

As a result of the strong oxidation process, the r-GO sheets were seriously damaged. The biobased graphene had a more complete lamellar structure than the r-GO. Clearly, the biobased graphene cannot match the r-GO in number of layers and purity. Further studies are needed to improve the quality of the biobased graphene.

Proposed Mechanisms Involved in Formation of Graphene

The proposed general mechanism of the iron catalyzed lignin based graphene is given below. Figure 8 gives the general proposed mechanism in the presence of iron particles. The main reactions were pyrolysis and carbonation of kraft lignin when the temperature was between 250 and 500 °C (Lv and Wu 2012). With the help of iron particles, polyolefin compounds are transformed to amorphous carbon (a-C) *via* catalytic dehydrogenation.

The a-C is in a metastable state, and with high energy content. Thus, a-C needs lower energy than C-atoms to dissolve into iron metal. Carbon dissolves into iron at temperatures higher than 570 °C. According to dissolve precipitate mechanism, it was proposed that a-C diffused into the metal particle at elevated temperatures followed by their precipitation as graphene on the free surface during the cool-down step as the solid solubility limit is reached (Schneider 2011). Given a small metallic particle and a long annealing time, the active carbon species migrate to the top surface and nucleate there (Zheng *et al*. 2010). As shown in Fig. 1, the graphene was observed for holding times in the range of 90 to 105 min. The areas with graphene were notably reduced, and for holding times > 105 min, less graphene was detected by Raman (Fig. 3). This may be due to a significant sp^2 carbon network expanding along the direction tangential to the surface of iron particles and accumulating through a graphite shell (Yu and Ye 2007; Wang *et al*. 2011).

As the temperature is increased, the a-C will have contact with the iron particles. Transformation of this part of a-C to graphite is a catalytic graphitization process. Iron can exhibit catalytic graphitization behavior at a low temperature (Sajitha *et al*. 2004). The decomposition of iron carbide plays a leading role during the insulation stage. The reaction equations are as follows:

$$Fe + C \rightarrow Fe_3C \quad (1)$$

$$Fe_3C \rightarrow Fe + C \quad (2)$$

New carbon generated by the decomposition of iron carbide is active and easily converted to graphite (Boehm 1973). However, adding too much iron may hinder the decomposition of Fe_3C. Hence, when the Fe/KL Ratio was 1:2, no 2D peak was detected (Fig. 2). Fe_3C is a weakly magnetic material at room temperature that is difficult to separate by magnet. Solid carbon source metal catalysis always use Cu and Ni films as the substrate. The factors associated with the quality of graphene are metal thickness and the solubility of C - atoms of the substrate itself. The synthesis of graphene involves two processes when using iron particles as catalyst. One is precipitation and dissolution of C atoms. The other is the formation and decomposition of iron carbide. Therefore, the formation of graphene also affected by the holding time.

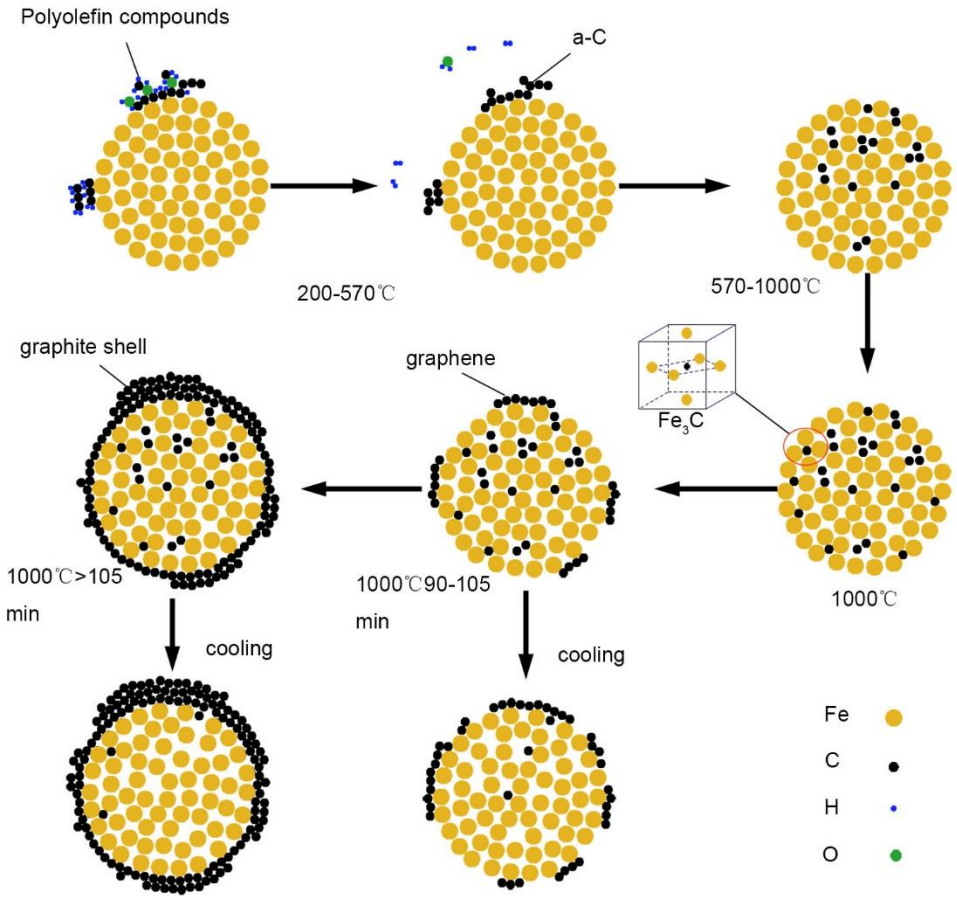

Fig. 8. Schematic diagram of the graphene synthesis routes from KL under the catalysis of iron particles

CONCLUSIONS

1. A biobased graphene from commercial kraft lignin was prepared in the presence of iron catalyst in this study. The characteristic structures of graphene nanosheets were confirmed by the FE-SEM, Raman spectroscopy, AFM, FTIR, and XRD analysis.
2. The preferable conditions for preparation of graphene nanosheets were evaluated. The produced graphene with better quality and less layers was obtained after thermal treatment for 90 min when the ratio of carbon source to iron was 3:1.
3. The folded lamellar graphene structure increased with the increase in holding time. Graphene sheets became agglomerative, and CNTs were obtained after thermally treated for 105 min.
4. AFM observation showed that thermal treatment of KL with iron particles yielded graphene with four to eight layers. FTIR spectra confirmed the formation of graphene-like materials. The produced graphite was multi-layered with a high degree of crystallization.

ACKNOWLEDGMENTS

The study was supported by Beijing Municipal Education Commission Co-building Project of Scientific Research and Postgraduate Training for Key Disciplines (2015), and National Natural Science Foundation of China (NSFC, No. 51572028).

REFERENCES CITED

Boehm, H. P. (1973). "Carbon from carbon monoxide disproportionation on nickel and iron catalysts: Morphological studies and possible growth mechanisms," *Carbon* 11(6), 583-586. DOI: 10.1016/0008-6223(73)90323-0.

Chen, S., Wu, Q., Mishra, C., Kang, J., Zhang, H., Cho, K., and Ruoff, R. S. (2012). "Thermal conductivity of isotopically modified graphene," *Nature Materials* 11(3), 203-207. DOI: 10.1038/nmat3207

Fan, Q., Lei, L., Yin, G., Chen, Y., and Sun, Y. (2014). "Direct growth of $FePO_4$/ graphene hybrids for Li-ion and Na-ion storage," *Electrochemistry Communications* 38, 120-123. DOI: 10.1016/j.elecom.2013.11.006

Fujita, J.-I., Ueki, R., Miyazawa, Y., and Ichihashi, T. (2009). "Graphitization at interface between amorphous carbon and liquid gallium for fabricating large area graphene sheets," *Journal of Vacuum Science & Technology B, Nanotechnology and Microelectronics: Materials, Processing, Measurement, and Phenomena* 27(6), 3063-3066. DOI: 10.1116/1.3253542

Juang, Z.-Y., Wu, C.-Y., Lo, C.-W., Chen, W.-Y., Huang, C.-F., Hwang, J.-C., Chen, F.-R., Leou, K.-C., and Tsai, C. H. (2009). "Synthesis of graphene on silicon carbide substrates at low temperature," *Carbon* 47(8), 2026-2031. DOI: 10.1016/j.carbon.2009.03.051

Kalita, G., Adhikari, S., Aryal, H. R., Umeno, M., Afre, R., Soga, T., and Sharon, M. (2008). "Fullerene (C_{60}) decoration in oxygen plasma treated multiwalled carbon nanotubes for photovoltaic application," *Applied Physics Letters* 92(6), 063508. DOI: 10.1063/1.2844881

Lee, D. H., Kim, J. E., Han, T. H., Hwang, J. W., Jeon, S., Choi, S.-Y., Hong, S. H., Lee, W. J., Ruoff, R. S., and Kim, S. O. (2010). "Versatile carbon hybrid films composed of vertical carbon nanotubes grown on mechanically compliant graphene films," *Advanced Materials* 22(11), 1247-1252. DOI: 10.1002/adma.200903063

Liang, T., Kong, Y., Chen, H., and Xu, M. (2016). "From solid carbon sources to graphene," *Chinese Journal of Chemistry* 34(1), 32-40. DOI: 10.1002/cjoc.201500429

Loh, K. P., Bao, Q., Eda, G., and Chhowalla, M. (2010). "Graphene oxide as a chemically tunable platform for optical applications," *Nature Chemistry* 2(12), 1015-1024. DOI: 10.1038/nchem.907

Lui, C. H., Liu, L., Mak, K. F., Flynn, G. W., and Heinz, T. F. (2009). "Ultraflat graphene," *Nature* 462(7271), 339-341. DOI: 10.1038/nature08569

Lv, G., and Wu, S. (2012). "Analytical pyrolysis studies of corn stalk and its three main components by TG-MS and Py-GC/MS," *Journal of Analytical and Applied Pyrolysis* 97, 11-18. DOI: 10.1016/j.jaap.2012.04.010

Mun, S. P., Cai, Z., and Zhang, J. (2013a). "Fe-catalyzed thermal conversion of sodium lignosulfonate to graphene," *Materials Letters* 100, 180-183. DOI:

10.1016/j.matlet.2013.02.101
Mun, S. P., Cai, Z., and Zhang, J. (2013b). "Magnetic separation of carbon-encapsulated Fe nanoparticles from thermally-treated wood char," *Materials Letters* 96, 5-7. DOI: 10.1016/j.matlet.2013.01.006
Novoselov, K. S., Jiang, D., Schedin, F., Booth, T. J., Khotkevich, V. V., Morozov, S. V., and Geim, A. K. (2005). "Two-dimensional atomic crystals," *Proceedings of the National Academy of Sciences of the United States of America* 102(30), 10451-10453. DOI: 10.1073/pnas.0502848102
Park, S., Lee, K.-S., Bozoklu, G., Cai, W., Nguyen, S. T., and Ruoff, R. S. (2008). "Graphene oxide papers modified by divalent ions—Enhancing mechanical properties *via* chemical cross-linking," *ACS Nano* 2(3), 572-578. DOI: 10.1021/nn700349a
Rafiee, M. A., Rafiee, J., Wang, Z., Song, H., Yu, Z.-Z., and Koratkar, N. (2009). "Enhanced mechanical properties of nanocomposites at low graphene content," *ACS Nano* 3(12), 3884-3890. DOI: 10.1021/nn9010472
Reina, A., Jia, X., Ho, J., Nezich, D., Son, H., Bulovic, V., Dresselhaus, M. S., and Kong, J. (2008). "Large area, few-layer graphene films on arbitrary substrates by chemical vapor deposition," *Nano Letters* 9(1), 30-35. DOI: 10.1021/nl801827v
Rodríguez-Manzo, J. A., Banhart, F., Terrones, M., Terrones, H., Grobert, N., Ajayan, P. M., Sumpter, B. G., Meunier, V., Wang, M., Bando, Y., and Golberg, D. (2009). "Heterojunctions between metals and carbon nanotubes as ultimate nanocontacts," *Proceedings of the National Academy of Sciences of the United States of America* 106(12), 4591-4595. DOI: 10.1073/pnas.0900960106
Rodríguez-Manzo, J. A., Pham-Huu, C., and Banhart, F. (2011). "Graphene growth by a metal-catalyzed solid-state transformation of amorphous carbon," *ACS Nano* 5(2), 1529-1534. DOI: 10.1021/nn103456z
Sajitha, E. P., Prasad, V., Subramanyam, S. V., Eto, S., Takai, K., and Enoki, T. (2004). "Synthesis and characteristics of iron nanoparticles in a carbon matrix along with the catalytic graphitization of amorphous carbon," *Carbon* 42(14), 2815-2820. DOI: 10.1016/j.carbon.2004.06.027
Schneider, J. J. (2011). "Transforming amorphous into crystalline carbon: Observing how graphene grows," *ChemCatChem* 3(7), 1119-1120. DOI: 10.1002/cctc.201100078
Shi, H., Barker, J., Saidi, M. Y., Koksbang, R., and Morris, L. (1997). "Graphite structure and lithium intercalation," *Journal of Power Sources* 68(2), 291-295. DOI: 10.1016/S0378-7753(96)02562-1
Si, Y., and Samulski, E. T. (2008). "Synthesis of water soluble graphene," *Nano Letters* 8(6), 1679-1682. DOI: 10.1021/nl080604h
Sun, Z., Yan, Z., Yao, J., Beitler, E., Zhu, Y., and Tour, J. M. (2010). "Growth of graphene from solid carbon sources," *Nature* 468(7323), 549-552. DOI: 10.1038/nature09579
Szabó, T., Berkesi, O., and Dékány, I. (2005). "DRIFT study of deuterium-exchanged graphite oxide," *Carbon* 43(15), 3186-3189. DOI: 10.1016/j.carbon.2005.07.013
Tan, P., Hu, C., Dong, J., Shen, W., and Zhang, B. (2001). "Polarization properties, high-order Raman spectra, and frequency asymmetry between stokes and anti-stokes scattering of Raman modes in a graphite whisker," *Physical Review B* 64(21), 214301. ISSN: 2469-9950
Thakur, V. K., Thakur, M. K., Raghavan, P., and Kessler, M. R. (2014). "Progress in green polymer composites from lignin for multifunctional applications: A review," *ACS Sustainable Chemistry & Engineering* 2(5), 1072-1092. DOI:

10.1021/sc500087z
Vallée, F., Gale, G. M., and Flytzanis, C. (1988). "Biphonon dynamics in ordered ammonium chloride," *Chemical Physics Letters* 149(5-6), 572-576. DOI: 10.1016/0009-2614(88)80385-3
Vlassiouk, I., Fulvio, P., Meyer, H., Lavrik, N., Dai, S., Datskos, P., and Smirnov, S. (2013). "Large scale atmospheric pressure chemical vapor deposition of graphene," *Carbon* 54, 58-67. DOI: 10.1016/j.carbon.2012.11.003
Wang, Y.-J., Wilkinson, D. P., and Zhang, J. (2011). "Noncarbon support materials for polymer electrolyte membrane fuel cell electrocatalysts," *Chemical Reviews* 111(12), 7625-7651. DOI: 10.1021/cr100060r
Wei, D., Liu, Y., Wang, Y., Zhang, H., Huang, L., and Yu, G. (2009). "Synthesis of N-doped graphene by chemical vapor deposition and its electrical properties," *Nano Letters* 9(5), 1752-1758. DOI: 10.1021/nl803279t
Yu, X., and Ye, S. (2007). "Recent advances in activity and durability enhancement of Pt/C catalytic cathode in PEMFC: Part I. Physico-chemical and electronic interaction between Pt and carbon support, and activity enhancement of Pt/C catalyst," *Journal of Power Sources* 172(1), 133-144. DOI: 10.1016/j.jpowsour.2007.07.049
Zhang, Y., Ren, L., Wang, S., Marathe, A., Chaudhuri, J., and Li, G. (2011). "Functionalization of graphene sheets through fullerene attachment," *Journal of Materials Chemistry* 21(14), 5386-5391. DOI: 10.1039/c1jm10257e
Zhao, W., Tan, P., Zhang, J., and Liu, J. (2010). "Charge transfer and optical phonon mixing in few-layer graphene chemically doped with sulfuric acid," *Physical Review B* 82(24), 245423. ISSN: 2469-9950
Zheng, M., Takei, K., Hsia, B., Fang, H., Zhang, X., Ferralis, N., Ko, H., Chueh, Y.-L., Zhang, Y., Maboudian, R., and Javey, A. (2010). "Metal-catalyzed crystallization of amorphous carbon to graphene," *Applied Physics Letters* 96(6), 063110. DOI: 10.1063/1.3318263

Article submitted: May 19, 2017; Peer review completed: July 15, 2017; Revised version received and accepted: July 18, 2017; Published: July 24, 2017.
DOI: 10.15376/biores.12.3.6545-6557